



HAL
open science

Soil order knowledge as a driver in soil properties estimation from Vis-NIR spectral data – Case study from northern Karnataka (India)

Subramanian Dharumarajan, Cécile Gomez, Manickam Lalitha, Beeman Kalaiselvi, Ramakrishnappa Vasundhara, R. Hegde

► To cite this version:

Subramanian Dharumarajan, Cécile Gomez, Manickam Lalitha, Beeman Kalaiselvi, Ramakrishnappa Vasundhara, et al.. Soil order knowledge as a driver in soil properties estimation from Vis-NIR spectral data – Case study from northern Karnataka (India). *Geoderma Régional*, 2023, 32, pp.e00596. 10.1016/j.geodrs.2022.e00596 . hal-03901428

HAL Id: hal-03901428

<https://hal.inrae.fr/hal-03901428>

Submitted on 17 Oct 2023

HAL is a multi-disciplinary open access archive for the deposit and dissemination of scientific research documents, whether they are published or not. The documents may come from teaching and research institutions in France or abroad, or from public or private research centers.

L'archive ouverte pluridisciplinaire **HAL**, est destinée au dépôt et à la diffusion de documents scientifiques de niveau recherche, publiés ou non, émanant des établissements d'enseignement et de recherche français ou étrangers, des laboratoires publics ou privés.

1 **Soil order knowledge as a driver in soil properties estimation from Vis-NIR spectral**
2 **data – Case study from Northern Karnataka (India)**

3
4 S. Dharumarajan*¹, C. Gomez^{2,3}, M. Lalitha¹, B. Kalaiselvi¹, R. Vasundhara¹, R. Hegde¹

5
6 ¹ICAR-National Bureau of Soil Survey and Land Use Planning, Regional Centre, Hebbal, Bangalore-560024

7 ²LISAH, Univ. Montpellier, IRD, INRAE, Institut Agro Montpellier, France

8 ³Indo-French Cell for Water Sciences, IRD, Indian Institute of Science, Bangalore, India

9 *sdharmag@gmail.com

10
11
12 **ABSTRACT**

13 Visible and near-infrared (Vis-NIR, 350-2500 nm) laboratory spectroscopy has been proven
14 to provide soil properties estimations, such as clay or organic carbon (OC). However, the
15 performances of such estimations may be dependent on pedological and spectral similarities
16 between calibration and validation datasets. The objective of this study was to analyse how
17 the soil order knowledge can be used to increase regression models performance for soil
18 properties estimation. For this purpose, Random Forest regression models were calibrated
19 and validated from both regional database (called regional models) and subsets stratified by
20 soil order from the regional database (called soil-order models). The regional database
21 contained 482 soil samples belonging to four soil orders (Alfisols, Vertisols, Inceptisols and
22 Entisols) and associated with Vis-NIR laboratory spectra and six soil properties: OC, sand,
23 silt, clay, cation exchange capacity (CEC) and pH. First, regional models provided i) high
24 accuracy of some soil properties estimations when considering the regional strategy in the
25 validation step (e.g., R^2_{val} of 0.74, 0.76 and 0.74 for clay, CEC and sand, respectively) but ii)
26 modest accuracy of these same soil properties when considering subsets stratified by soil
27 order from the regional database in validation step (e.g., R^2_{val} of 0.48, 0.58 and 0.38 over
28 Vertisol for clay, CEC and sand, respectively). So the estimation accuracy appreciation is
29 highly depending on the validation database as there is a risk of over-appreciated prediction

30 accuracies at the soil-order scale when figures of merit are based on a regional validation
31 dataset. Second, this work highlighted that the benefit of a soil-order model compared to a
32 regional model for calibration depends on both soil property and soil order. So no
33 recommendations for choosing between both models for calibration may be given. Finally,
34 while Vis-NIR laboratory spectroscopy is becoming a popular way to estimate soil
35 physicochemical properties worldwide, this work highlights that this technique may be used
36 discreetly depending on the targeted scale and targeted soil type.

37

38 Key words: Visible Near-infrared, regional model, soil-order model, random forest, soil
39 variability, prediction accuracy

40

41

42 **1. Introduction**

43 Visible and near-infrared (Vis-NIR, 350–2500 nm) laboratory spectroscopy provides a
44 complementary method to wet chemistry methods for estimating soil properties (e.g.,
45 [Viscarra Rossel et al., 2006](#); [Demattê et al., 2004](#); [Stenberg et al., 2010](#); [McBride et al., 2022](#))
46 and is non-destructive, rapid, low-cost, efficient, repeatable and reproducible with an
47 acceptable degree of accuracy. Soil reflectance in the 350–2500 nm spectral region is the
48 result of soil physical, chemical, and mineralogical properties and their compositions ([Ben-](#)
49 [Dor, 2002](#); [Stenberg et al., 2010](#)) as the soil spectrum is composed of absorption features of
50 chemical constituents (e.g., absorption of OH of water molecules) and overall spectral shape
51 of the physical properties (e.g., texture) ([Ben-Dor and Banin, 1995a, 1995b](#)). As explained
52 by [Chabrillat et al. \(2019\)](#) a targeted soil property can be estimated accurately from Vis-NIR
53 data if this targeted property follows the following rules: ‘Rule (1.1) the soil property S_i has a
54 specific spectral signature due to a chemical or physical structure (e.g., OH- ion for clay) or

55 Rule (1.2) the soil property S_i is correlated with a soil property S_j having a specific spectral
56 signature due to an associated chemical or physical structure (e.g., cation exchange capacity
57 –CEC- correlated with clay content) (Ben-Dor et al., 2002); and additionally, Rule (1.3) the
58 soil property S_i has to have a quite high amount of variability (Gomez et al., 2012a, b)'.
59

60 Soil properties are estimated from laboratory Vis-NIR spectroscopy using regression
61 models, such as stepwise multilinear regression (Leone et al., 2012), multivariate adaptive
62 regression splines (Bilgili et al., 2010), memory-based learning (Jaconi et al., 2019; Ng et al.,
63 2022), Partial Least Square Regression (PLSR, Viscarra Rossel and Behrens, 2009; Gupta et
64 al., 2018; Davari et al., 2021), cubist (Viscarra Rossel et al., 2016) and support vector
65 machine (SVM, Stevens et al., 2010; Naibo et al., 2022) and random forest (RF, Hobbey and
66 Prater, 2019; Bao et al., 2020; Dharumarajan et al., 2022). Nawar and Mouazen (2019) used
67 the RF model to compare the efficacy of in situ and field Vis-NIR spectroscopy on the
68 estimation of soil properties and confirmed that the RF model could capture maximum
69 variability ($R^2=0.65-0.75$) under both conditions. Morellos et al. (2016) reported that machine
70 learning techniques, such as RF, are capable of making spectral variable selections more
71 efficiently compared with PLSR. Ghasemi and Tavakoli (2013) studied the performance of
72 the RF algorithm on Vis-NIR spectroscopy with PLSR and nonlinear SVM and concluded
73 that RF performed well and has the potential for modelling linear and nonlinear multivariate
74 calibrations.

75 For more than two decades, Vis-NIR laboratory spectroscopy has been extensively
76 explored in various pedological contexts and based on these regression models to estimate
77 various soil properties, such as pH (e.g., Shepherd and Walsh, 2002), soil organic carbon
78 (SOC) (e.g., Bellon-Maurel et al., 2011; Hedley et al., 2015), texture or particle size fractions
(e.g., Gomez et al., 2008), CEC (e.g., Shepherd and Walsh, 2002), exchangeable bases (e.g.,

79 [Pinheiro et al., 2017](#)), available nutrients (e.g., [Cozzolino and Moron, 2003](#); [Terra et al.,](#)
80 [2015](#)) and soil salinity (e.g., [Farifteh et al., 2008](#)).

81 Based on the high potential of this technique, Vis-NIR soil spectral libraries covering
82 different extent (local, regional, country, continental, and global extents) have been
83 developed these later years ([Shepherd and Walsh, 2006](#); [Vasques et al., 2008](#); [Stevens et al.,](#)
84 [2013](#); [Viscarra Rossel et al., 2016](#)). Large soil spectral libraries contain information from a
85 wide variety of soils and benefit from a large range of contents for the targeted soil
86 properties and correlations between soil properties, but they rarely reflect local specificities
87 ([Stevens et al., 2013](#); [Gogé et al., 2014](#)) unless they include a high density of spatial
88 sampling ([Viscarra Rossel et al., 2016](#)). Numerous studies showed that estimations of soil
89 properties over local areas using a large library can be improved by selecting an appropriate
90 “local” subset from the large library to be used in the calibration step ([Zeng et al., 2016](#)).
91 Several ways have been developed to build an “appropriate local subset” based on large
92 libraries and calibrate regression models, such as considering calibration datasets constituted
93 a subset of the large libraries based on i) the geographical locations which have to be close
94 to the validation subset (e.g., [Guerrero et al., 2010](#); [Shi et al., 2015](#)), ii) their spectral
95 similarity with the local spectra (e.g., [Wetterlind and Stenberg, 2010](#), [Gogé et al., 2012](#);
96 [Nocita et al., 2014](#)) or iii) environmental covariates similar to one of the local targeted
97 samples, such as parent material (e.g., [Peng et al., 2013](#); [Xu et al., 2016](#)) and land use type
98 (e.g., [Zeng et al., 2016](#)). An additional procedure, called “spiking”, considered calibration
99 datasets constituted by both the large library and a subset of local samples (e.g., [Brown,](#)
100 [2007](#); [Sankey et al., 2008](#); [Nawar and Mouazen, 2017](#)).

101 While some studies have highlighted that local models (e.g., based on land use, parent
102 material or soil groups) may outperform regional models (e.g., [Vasques et al., 2010](#); [Liu et](#)
103 [al., 2018](#)), the literature also contains studies showing that local models may not exhibit any

104 advantages over regional models (e.g., [Madari et al., 2005](#); [McDowell et al., 2012](#)). For
105 example, [Zeng et al. \(2016\)](#) obtained better soil organic matter predictions for uplands based
106 on local models (using calibration data restricted to land use types or spectral similarity) in
107 comparison with regional models (using calibration data from a regional spectral library);
108 inversely, they obtained better performances for paddy lands based on “regional” models
109 compared to local models. [Gomez and Coulouma \(2018\)](#) showed that prediction models built
110 at a regional database yielded good performances when they were validated at the same
111 regional extent but poor to good performances when they were validated at a local extent
112 (within-field in their case), depending on the model robustness.

113 In this context, the objective of this study was to analyze how the soil order
114 knowledge can be used to increase regression models performance for soil properties
115 estimation. Models were calibrated and validated from both regional database (regional
116 model) and subsets stratified by soil order from the regional database (soil-order model). This
117 work used a soil spectral library composed of 482 soil samples collected from the northern
118 Karnataka Plateau in India, which is characterized by four soil orders.

119

120

121 **2. Materials and methods**

122 **2.1. Study area**

123 The study area extends across seven sub-watersheds belonging to five districts of Karnataka
124 (Gulbarga, Koppal, Yadgir, Bidar and Gadag, [Table 1](#)) representing the northern Karnataka
125 Plateau region ([Fig. 1](#)). These sub-watersheds cover an area from 1603 ha to 68131 ha. They
126 experience semiarid climatic conditions with average annual rainfall and temperature of 633-
127 866 mm and 22-33° C, respectively and is considered drought-prone. With the exception of
128 August and September, the potential evapotranspiration exceeds the rainfall occurrence

129 throughout the year. Predominantly, the seven sub-watersheds have the geology of the
 130 peninsular gneiss, basalt and schists. The length of the growing period across the studied area
 131 varied from <90 days for the Koppal district to 120-150 days for the Yadgir, Kalburgi, and
 132 Gadag districts. The major crops grown in the area are sorghum (*Sorghum bicolor*), maize
 133 (*Zea mays L*), cotton (*Gossypium sp.*), sunflower (*Helianthus annuus*), groundnut (*Arachis*
 134 *hypogaea*), red gram (*Cajanus cajan*), mango (*Mangifera indica*), pomegranate (*Punica*
 135 *granatum*), marigold (*Tagetes sp.*) and sapota (*Manilkara zapota*) under rainfed conditions.
 136 The sequence of dominant soil orders in the northern Karnataka Plateau is Alfisols,
 137 Inceptisols, Vertisols and Entisols (NBSS&LUP, 1998), based on the USDA classification
 138 system.

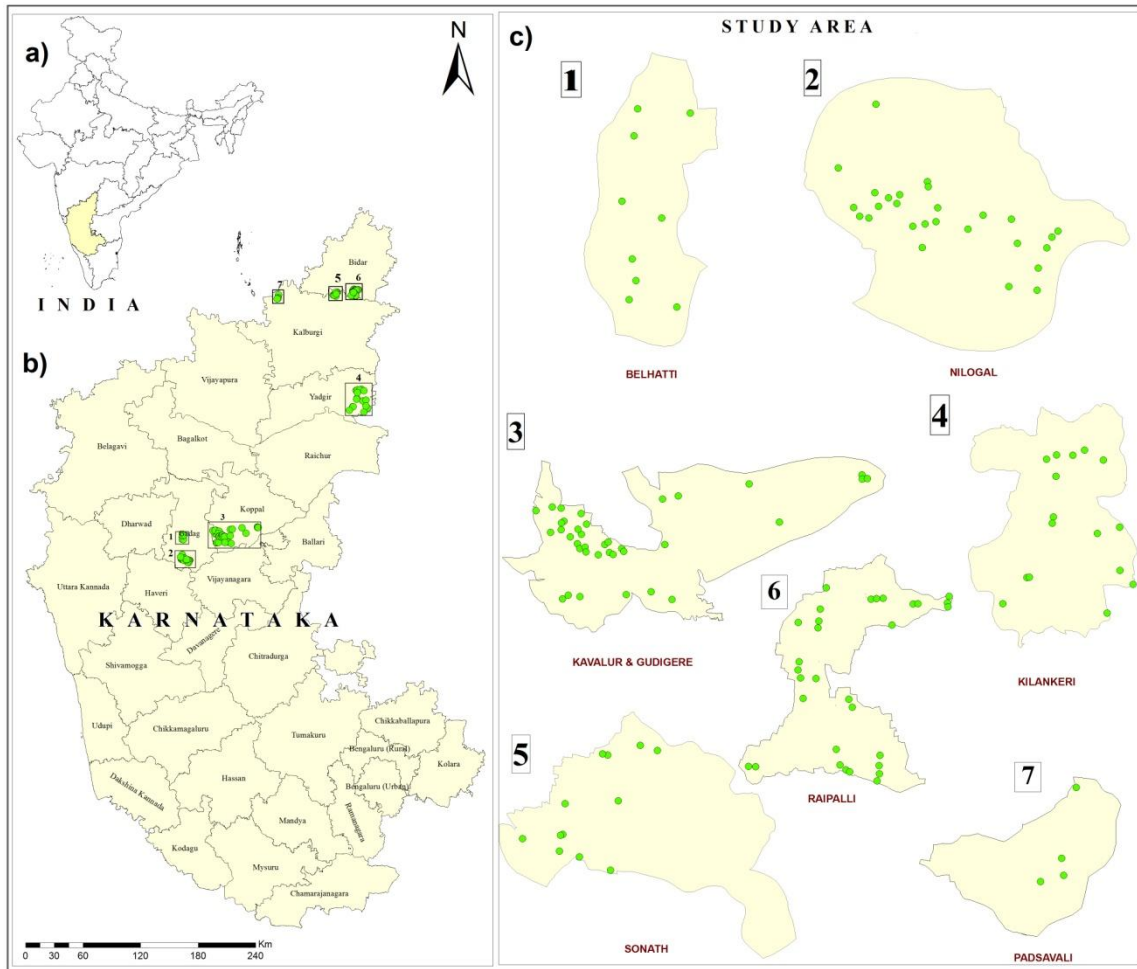
139

140

141 **Table. 1. Description of the seven sub-watersheds**

District name	Sub-watershed name	Location		Area (ha)	Number of profiles
Gadag	Belhatti	75.63° E	15.31° N	1603	9
		75.58° E	15.24° N		
	Nilogal	75.69° E	15.13° N	10744	27
		75.58° E	15.02° N		
Koppal	Kavalur & Gudigere	76.34° E	15.49° N	68131	40
		75.87° E	15.16° N		
Yadgir	Kilankeri	77.48° E	16.80° N	60106	16
Bidar	Raipalli	77.15° E	16.48° N	3059	31
		77.27° E	17.69° N		
	Sonath	77.20° E	17.62° N	3875	12
		77.10° E	17.67° N		
Gulburga	Padsavali	77.02° E	17.59° N	2873	4
		76.49° E	17.62° N		
		76.42° E	17.57° N		

142



143

144 **Fig. 1.** Location of a) the Karnataka state in India, b) the seven sub-watersheds (black
 145 rectangles) over the state of Karnataka and c) the soil profile (green points) over each seven
 146 sub-watershed.

147

148

149 2.2 Datasets

150 Soil profiles collected under the Sujala III project (Hegde et al., 2018) were used for the
 151 present study. A total of 139 soil profiles were selected and dug until the hard rock was
 152 reached or up to 2 m, whichever occurred first based on the landform, slope and land use
 153 variability (Fig. 1b and c). The Belhatti, Nilogal, Kavalur & Gudigere, Kilankeri, Raipalli,
 154 Sonath, Padsavali sub-watersheds contain 9, 27, 40, 16, 31, 12, 4 soil profiles, respectively
 155 (Table 1) and the number of profiles depends on soil variability in the sub-watershed.

156 Horizon-wise soil samples (a total of 482 samples) were collected, air-dried, sieved through a
157 2 mm sieve and analyzed for soil properties. The studied soils were taxonomically grouped
158 into soil orders, namely, Vertisols (20 profiles, 82 samples), Alfisols (59 profiles, 217
159 samples), Inceptisols (44 profiles, 152 samples) and Entisols (16 profiles, 31 samples), based
160 on their morphological characteristics ([Soil survey staff, 2014](#)). Dominant soil characteristics
161 of different soil orders are presented in [supplementary information 1](#).

162 The samples were analyzed for particle-size distribution by the International Pipette
163 method ([Richards, 1954](#)), and OC was estimated by the [Walkley and Black \(1934\)](#) method.
164 Soil pH in 1:2.5 soil : water suspension and cation exchange capacity (CEC) were determined
165 as described by [Jackson \(1973\)](#). The 482 samples constituted the regional dataset, while the
166 samples stratified by soil order constituted four subsets (one subset per soil order). The
167 correlation between soil properties were analysed using Pearson correlation coefficient.

168

169 **2.3 Spectral data acquisition**

170 An ASD pro-FR Portable Spectroradiometer (Analytical Spectral Devices Inc., Boulder, CO,
171 USA) was used to measure the Vis-NIR spectral data of the soils under laboratory conditions.
172 The processed soil samples (sieved and dried) were illuminated with four tungsten quartz
173 halogen lamps that were fixed at an angle of 36°. The soil spectral reflectance was recorded
174 with a field of view of 8° using a pistol grip. Between 350 and 1000 nm, the spectral
175 sampling interval of the ASD spectrometer was originally 1.4 nm for a spectral resolution of
176 3 nm, while from 1000 to 2500 nm, the spectral sampling interval was originally 2 nm for a
177 spectral resolution of 10 nm. The reflectance was oversampled by the ASD software to 1 nm
178 in both spectral ranges, leading to a total number of spectral bands of 2151. White reference
179 spectra were measured with a Spectralon® standard white panel after every 5 samples. A

180 representative spectrum for each soil sample was obtained by the mean of measurements of
181 the individual samples in triplicate.

182 **2.4. Preprocessing of spectral data**

183 Spectral data were pre-processed to correct for background effects and light scattering and to
184 omit nonlinearities in the spectra (e.g., [Nocita et al., 2013](#); [Babaeian et al., 2015](#)). The
185 spectral absorbance obtained at ranges of 350-400 nm and 2450-2500 nm were removed to
186 eliminate noises. All spectral data were first transformed into pseudo absorbance (log
187 [1/reflectance]) values to achieve linearization between the spectra and soil properties by
188 highlighting the edges of absorption ([Stenberg et al., 2010](#)). Then, the Savitzky–Golay filter
189 was applied to eliminate high-frequency noise and pass low-frequency signals to achieve
190 smooth soil spectra ([Delwiche, 2010](#)). This filter fits successive subsets (windows) of
191 adjacent data points (7 nm) with a low-degree polynomial through the use of linear least
192 squares.

193

194 **2.5 Spectroscopic modelling**

195 Random forest regression (RF) was used for soil property predictions from Vis-NIR spectra.
196 The RF regression works on the principle of assemblages of a number of decision trees where
197 random vectors are independently selected and equally distributed among all the trees
198 ([Breiman, 2001](#); [Zeraatpisheh et al., 2021](#)). The number of trees (n_{tree}), minimum number of
199 samples at the terminal node n_{min} and the number of predictors used for fitting the tree (M_{try})
200 are the three parameters that decide the fitting of RF. A Random Forest 4.6 package in an R
201 environment was used for the estimation of soil properties. The RF parameters were
202 optimised using the *tune* function, and the parameters used for running the model are
203 presented in [Supplementary Information 2](#). The accuracy of the model is set by the mean

204 square error (MSE_{OOB}) of the aggregated out-of-bag (OOB) predictions generated from the
205 bootstrap subset and is calculated as follows:

$$206 \quad MSE_{OOB} = n^{-1} \sum_{i=1}^n (z_i - \hat{z}_i^{OOB})^2 \quad (1)$$

207 where n is the number of observations, z_i is the average prediction of the i^{th}
208 observation and \hat{z}_i^{OOB} is the average prediction for the i^{th} observation from all trees for which
209 the observation was OOB.

210

211 **2.6 Bootstrap procedure**

212 A bootstrap procedure was applied to each dataset (the entire dataset and the four subsets
213 stratified by soil order) to define N sets of calibration and validation subsets, where N is equal
214 to 50 (Efron and Tibshirani, 1993). Bootstrapping involved repeated random sampling for
215 calibration and validation data. Each subset stratified by soil order was divided randomly into
216 thirds; two third of the subset was used for calibration (providing four calibration subsets
217 called *BD_cal_Ver*, *BD_cal_Alf*, *BD_cal_Inc* and *BD_cal_Ent*) and one third of the subset
218 was used for validation (providing four validation subsets called *BD_val_Ver*, *BD_val_Alf*,
219 *BD_val_Inc* and *BD_val_Ent*) (Fig. 2). Then, these four calibration subsets and four
220 validation subsets were aggregated to constitute the *BD_Cal_Regional* dataset containing 328
221 samples and the *BD_Val_Regional* dataset containing 154 samples, respectively (Fig. 2).

222 For each bootstrap iteration, a regional RF model was fitted for predicting each soil
223 property, based on the *BD_Cal_Regional* and validated using the *BD_Val_Regional* dataset
224 and the four validation subsets stratified by soil order (*BD_val_Ver*, *BD_val_Alf*, *BD_val_Inc*
225 and *BD_val_Ent*). As well, for each bootstrap iteration, a soil-order RF model for each soil
226 property was built based on each calibration subset stratified by soil order (*BD_cal_Ver*,
227 *BD_cal_Alf*, *BD_cal_Inc* and *BD_cal_Ent*) and validated on the validation data of the same
228 order.

229

230

231

232 **2.7 Model evaluation**

233 The performance of the RF models was evaluated based on the 50 iterations for each
234 validation dataset using four accuracy estimates (Bellon-Maurel et al., 2010), the coefficient
235 of determination (R^2_{val}), root mean square error ($RMSE_{val}$), mean error (ME_{val}), and ratio of
236 performance to interquartile distance ($RPIQ_{val}$), based on the following equations:

$$237 \quad R^2_{val} = 1 - \frac{\sum_{i=1}^n (p_i - o_i)^2}{\sum_{i=1}^n (o_i - \bar{o}_i)^2} \quad (2)$$

$$238 \quad ME_{val} = \frac{1}{n} \sum_{i=1}^n (o_i - p_i) \quad (3)$$

$$239 \quad RMSE_{val} = \sqrt{\frac{1}{n} \sum_{i=1}^n (o_i - p_i)^2} \quad (4)$$

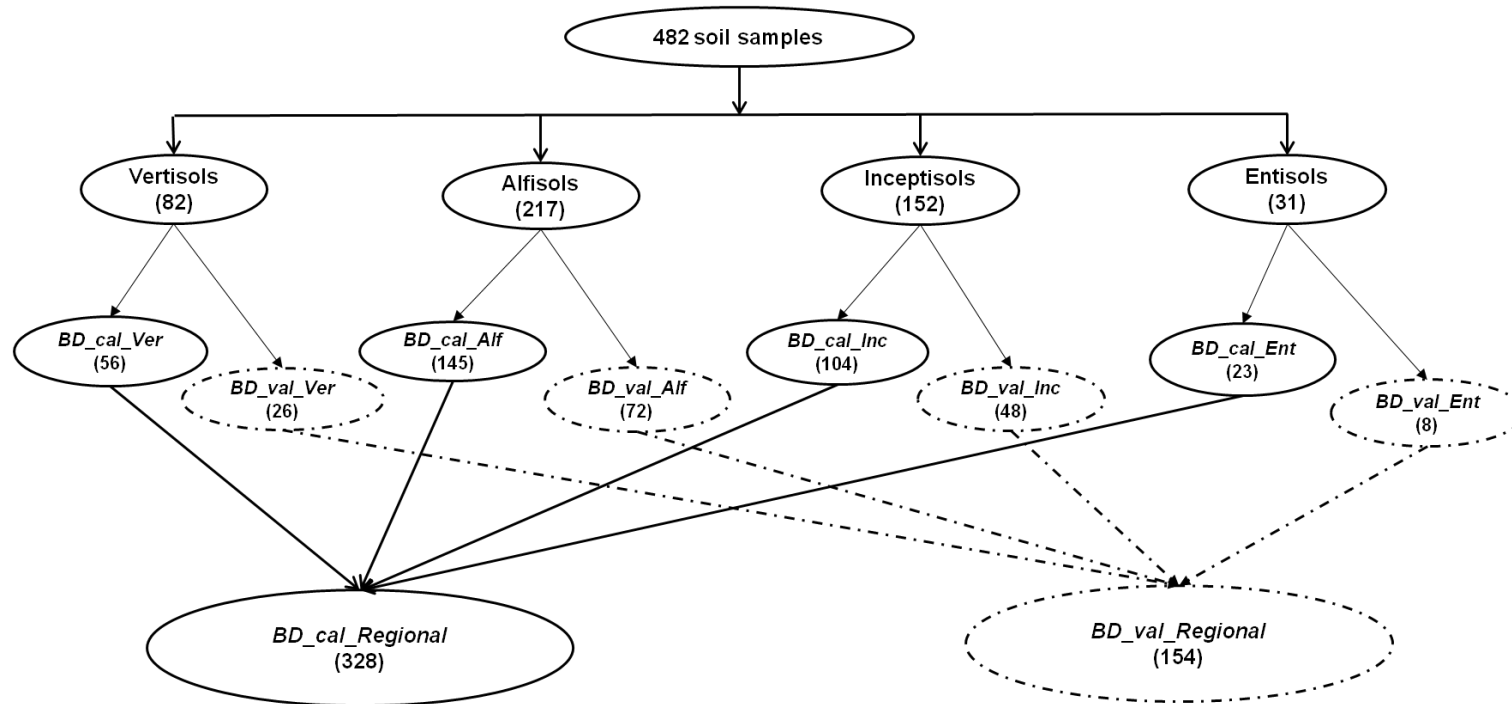
240 where p_i and o_i are the predicted and observed values, respectively and \bar{o}_i is the means of the
241 observed values.

$$242 \quad RPIQ_{val} = \frac{IQ}{RMSE_{val}} \quad (5)$$

243 where IQ is the difference between the third quartile Q3 and the first quartile Q1. A larger
244 RPIQ value indicates improved model performance. The reliability of the prediction was
245 evaluated based on the RPIQ, for which a RPIQ lower than 1.5 may be consider as a poor
246 performance, RPIQ from 1.5 to 3.0 may be consider as a acceptable performance, and RPIQ
247 up to 3.0 may be consider as a good performance (Veum et al., 2015).

248

249



250

251 **Fig. 2.** Construction of calibration and validation datasets for regional and soil-order models (number of samples in parentheses)

252

253 **3. Results**

254 **3.1 Preliminary analysis of soil properties and spectra**

255 *3.1.1 Based on the entire dataset*

256 The clay, sand and silt of the entire soil dataset (482 samples) ranged from 1.2 to 77.2%, 2.7
257 to 93.4% and 2.4 to 39.4%, respectively, with means of 42.8, 40.8 and 16.3%, respectively
258 (Table 2). The soil pH ranged from 4.7 to 11.2 with mean of 8.0. The SOC content ranged
259 from 0.03 to 1.6% with a mean of 0.6%. The mean CEC of the northern Karnataka Plateau
260 soils was 29.5 cmol (+) kg⁻¹, with a 66.4% coefficient of variation.

261 Based on the entire soil dataset, clay had a high negative correlation with sand ($r = -$
262 0.95), a high positive correlation with CEC ($r = 0.71$) and a modest correlation with silt ($r =$
263 0.42) (Supplementary Information 3). Sand had a high negative correlation with silt ($r = -$
264 0.68). CEC had a positive correlation with silt ($r = 0.64$) and a negative correlation with sand
265 ($r = -0.79$). Finally, no correlations existed between the other properties of the overall soil
266 dataset. The sand content was positively correlated with the average reflectance along the
267 Vis-NIR spectral range, while the clay content was negatively correlated with the average
268 reflectance along the Vis-NIR spectral range (Fig. 3). The CEC and silt content also followed
269 correlation patterns similar to clay along the Vis-NIR spectral range. Finally, there was no
270 significant correlation between pH and OC with the average reflectance.

271

272

273

274

275

276

277 Table 2. Statistical summary of soil properties for the entire dataset and each subset stratified
 278 per soil order.

		sand (%)	silt (%)	clay (%)	pH	SOC (%)	CEC (cmol (+) kg ⁻¹)
Entire samples (N=482)	Min	2.7	2.4	1.2	4.7	0.03	1.7
	Max	93.4	39.4	77.2	11.2	1.60	80.9
	Mean	40.8	16.3	42.8	8.0	0.58	29.5
	SD	23.4	7.9	19.0	1.1	0.27	19.6
	CV (%)	57.4	48.5	44.4	13.8	47.5	66.4
Vertisols (N=82)	Min	2.7	10.5	37.7	6.7	0.16	10.2
	Max	51.8	36.5	77.2	9.5	1.29	80.9
	Mean	15.5	22.1	62.4	8.5	0.59	51.5
	SD	10.6	5.2	8.75	0.6	0.25	17.9
	CV (%)	68.4	23.4	14.0	6.6	43.1	34.8
Alfisols (N=217)	Min	6.3	2.4	2.3	4.7	0.12	1.7
	Max	93.4	34.5	76.1	9.9	1.55	54.0
	Mean	49.3	12.0	38.6	7.5	0.56	18.1
	SD	19.3	6.2	17.7	1.1	0.26	9.8
	CV (%)	39.2	51.6	45.9	14.7	46.2	54.1
Inceptisols (N=152)	Min	3.2	3.8	4.6	5.4	0.08	3.4
	Max	88.4	37.9	73.3	11.2	1.26	80.4
	Mean	39.8	19.2	41.1	8.6	0.55	35.4
	SD	22.5	7.2	18.0	1.0	0.28	18.8
	CV (%)	56.5	37.5	43.8	11.6	51.0	53.1
Entisols (N=31)	Min	9.97	2.6	1.2	6.0	0.03	2.03
	Max	94.0	39.4	58.3	8.7	1.60	51.9
	Mean	53.2	17.6	29.1	7.6	0.61	21.5
	SD	28.0	10.6	18.3	0.8	0.33	16.7
	CV (%)	52.8	60.2	62.9	10.7	52.4	77.7

279

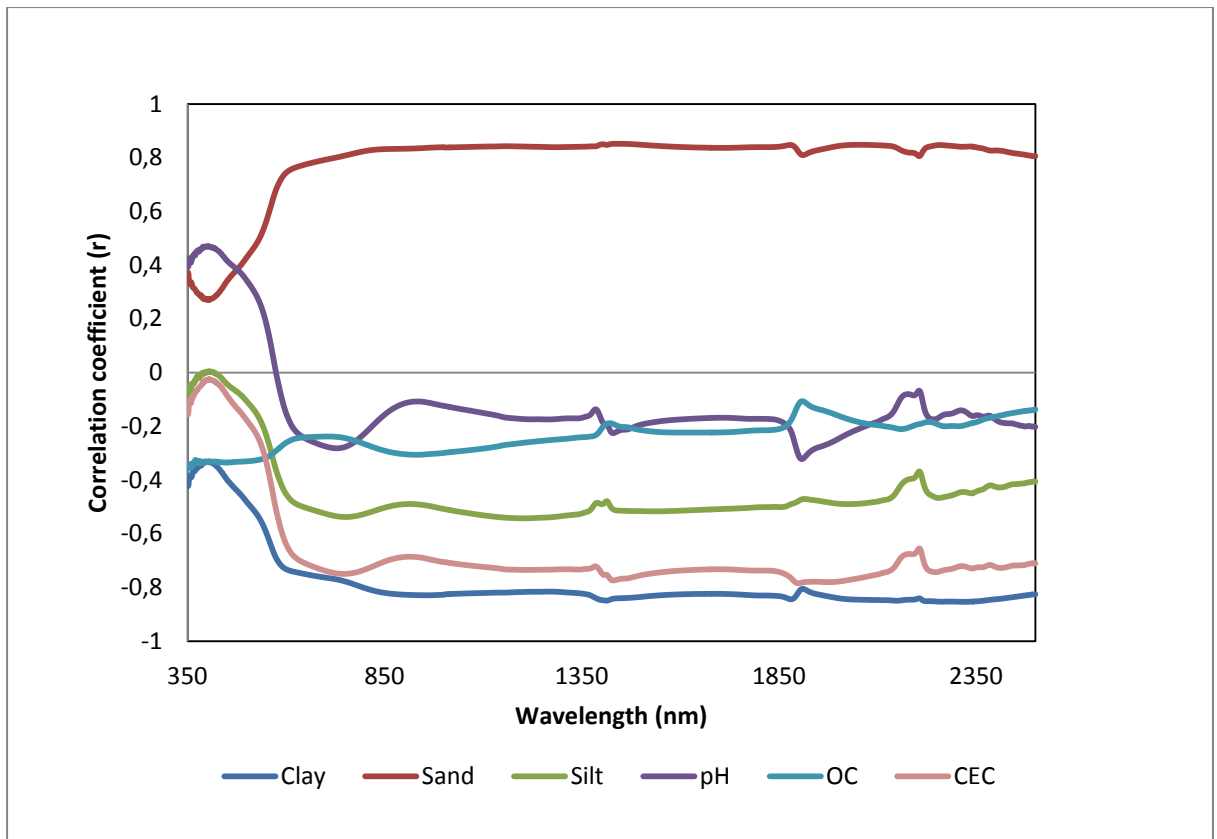
280

281

282

283

284



285

286

Fig. 3. Correlation coefficient (r) between soil properties and mean reflectance at each wavelength based on the entire dataset.

287

288

289

290 3.1.2 Based on subsets stratified per soil order

291 The Vertisols and Inceptisols were characterized by a higher content of clay (mean > 40%),

292 CEC (mean > 35 cmol (+) kg⁻¹) and pH (mean > 8.5) than Alfisols and Entisols (Table 2).

293 The high CEC in Vertisols and Inceptisols may be due to the presence of highly weatherable

294 minerals derived from basaltic parent materials and these soils have abundant 2:1 type clay

295 minerals. The Alfisols and Entisols were characterized by high contents of sand (mean >

296 49%) and CEC (mean of 18.1 and 21.5 cmol (+) kg⁻¹, respectively). The SOC range and

297 distribution were similar from one soil order to another (Table 2).

298 Regardless of the soil order, clay had a high negative correlation ($r < -0.87$) with sand
299 (Supplementary Information 4 to 7). Clay and CEC had a high positive correlation in
300 Inceptisols and Entisols ($r > 0.89$) and a modest correlation in Alfisols and Vertisols (r from
301 0.43 to 0.46). Clay and silt were highly correlated in Entisols ($r = 0.85$), slightly correlated in
302 Inceptisols ($r = 0.50$), and had no correlation in either of the other soil orders. OC and pH had
303 a modest negative correlation in Vertisols and Inceptisols (r of -0.57 and -0.56, respectively)
304 and poor correlations in the other soil orders.

305 3.1.3 Vis-NIR spectra per soil order

306 The mean spectra measured for Entisols and Alfisols presented the highest absorption band
307 centred at 2207 nm (Fig. 4), which corresponds to the combination of OH stretching and OH-
308 Al bending modes observed in clay (Chabrilat et al., 2002). Vertisols recorded relatively
309 poor reflectance irrespective of the bandwidth, which might be due to the presence of
310 smectite clay minerals in Vertisols and high moisture-holding capacities (Baumgardner et al.,
311 1985; Demattê et al., 2017). The higher reflectance of Entisols and Alfisols might be
312 attributed to the predominance of highly weatherable minerals (Poppiel et al., 2018) and sand
313 contents (Viscarra Rossel et al., 2006) which may have increased their albedo. Alfisols and
314 Entisols had broad absorption features between 850-1100 nm related to the specific
315 absorption shoulder of goethite and haematite (Srivastava et al., 2004). These particular iron
316 oxide absorption bands were not observed in the reflectance spectra of other soil orders
317 because iron oxides are underdeveloped in Inceptisols and Vertisols (Poppiel et al., 2018).

318

319

320

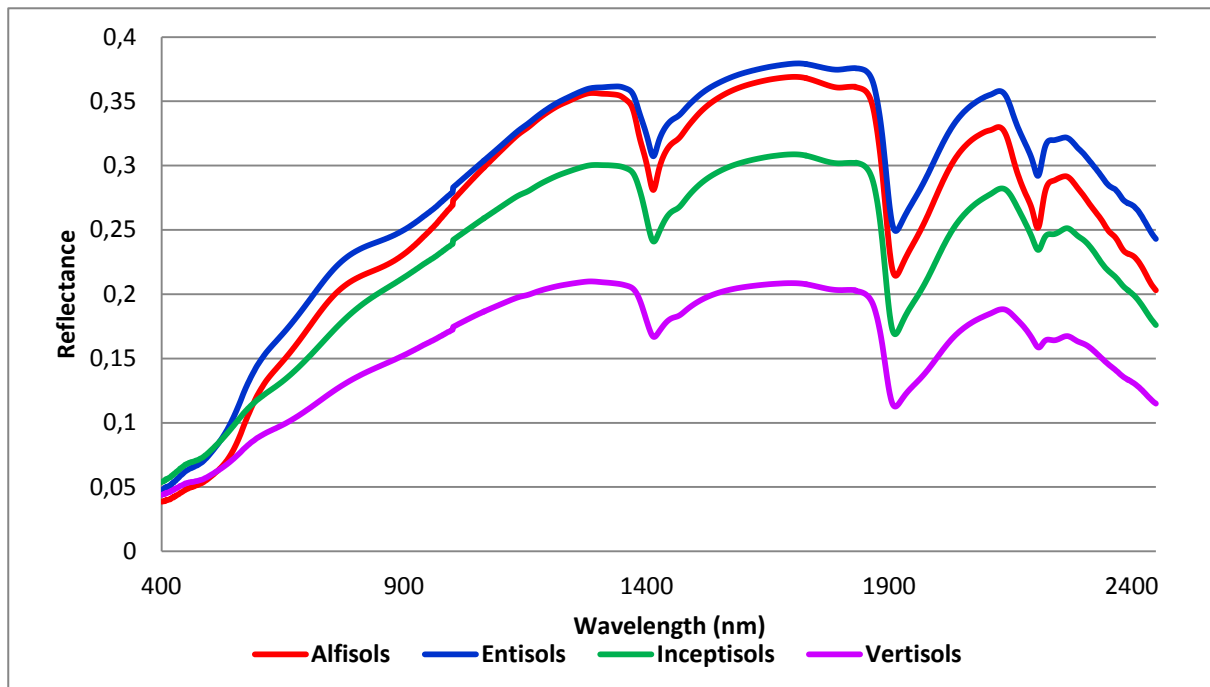


Fig. 4. Mean spectral reflectance of soil samples stratified per soil order.

321
322
323

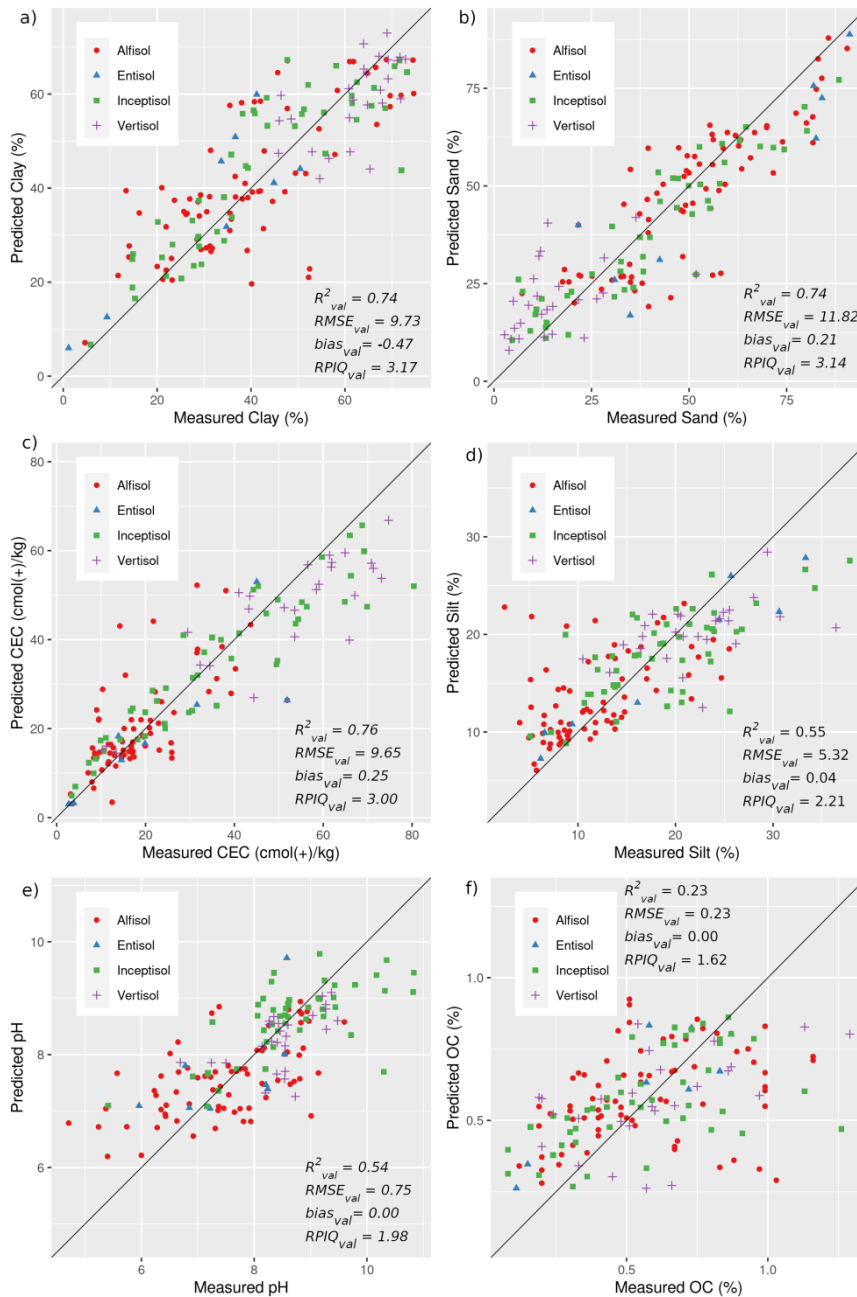
324

325 3.2 Prediction performance of regional models

326 3.2.1. Analysis based on the entire database

327 Fifty regional models were built from a *BD_Cal_Regional* dataset for each soil property and
 328 validated using a *BD_Val_Regional* dataset. The RF regional models for CEC estimates
 329 provided good performances, with R^2_{val} and $RPIQ_{val}$ values of 0.76 and 3.00, respectively
 330 (Fig. 5c), as the RF regional models for clay and sand which provided good performances
 331 with R^2_{val} values of 0.74 and $RPIQ_{val}$ values of 3.17 and 3.14, respectively (Fig. 5a and b).
 332 The RF regional models for silt and pH estimates provided modest performances, with R^2_{val}
 333 and $RPIQ_{val}$ values above 0.5 and 1.5, respectively (Fig. 5d and e). Finally, the regional
 334 models for SOC estimates yielded poor performances, with R^2_{val} value lower than 0.5 (Fig.
 335 5f). The variations in performances based on 50 iterations (standard deviation) were modest,
 336 regardless of the studied soil property (Supplementary Information 8).

337



338

339 **Fig. 5.** Scatter plots of predicted versus observed soil properties obtained for the

340

BD_Val_Regional datasets.

341

342 3.2.2. Analysis based on the soil order subsets

343 The 50 regional models built from the samples of *BD_Cal_Regional* for each soil property

344 were then tested on samples of specific soil orders: *BD_val_Ver*, *BD_val_Alf*, *BD_val_Inc*,

345 *BD_val_Ent*. While the regional models for clay and sand prediction provided good

346 performances over the entire dataset (Fig. 5a and b), both models yielded acceptable ($R^2_{val} >$

347 0.50, $RPIQ_{val} > 1.50$) to good ($R^2_{val} > 0.70$, $RPIQ_{val} > 3.00$) performances for soil samples
348 belonging to Alfisols, Inceptisols and Entisols (Table 3, Fig. 5a and b) and poor performances
349 for Vertisols ($R^2_{val} < 0.50$, Table 3, purple points on Fig. 5a and b), which were characterized
350 by the smallest clay and sand ranges among the four soil orders (SD of 8.75% and 10.6%,
351 respectively, Table 2). Additionally, while the regional models for CEC prediction provided
352 good performances over the entire dataset (Fig. 5c), it yielded acceptable ($R^2_{val} > 0.50$,
353 $RPIQ_{val} > 1.50$) performances for Vertisols (Table 3, purple points on Fig. 5c), good
354 performances ($R^2_{val} > 0.70$, $RPIQ_{val} > 3.00$) for Inceptisols and Entisols (Table 3, green and
355 blue points in Fig. 5c) and poor performances for Alfisols (Table 3, red points on Fig. 5c).

356 The regional models for silt prediction yielded acceptable ($R^2_{val} > 0.50$,
357 $RPIQ_{val} > 1.50$) to good ($R^2_{val} > 0.70$, $RPIQ_{val} > 3.00$) performances for soil samples belonging
358 to Inceptisols and Entisols (Table 3, Fig. 5d), but performed poorly over Vertisols and
359 Alfisols (Table 3, Fig. 5d) where the silt range was small (SD of 5.2 and 6.2%, respectively,
360 Table 2). Finally, the regional models for the prediction of pH and SOC yielded poor
361 performances regardless of the soil order (Table 3, Fig. 5e and f). Therefore, although the
362 regional models for pH prediction provided acceptable performances over the entire dataset
363 (Fig. 5e), it did not provide accurate predictions at the soil-order level (Table 3).

364

365 3.3 Prediction performance of soil-order model

366 Fifty soil-order models were built from calibration samples of each soil order (*BD_Cal_Ver*,
367 *BD_Cal_Alf*, *BD_Cal_Inc* and *BD_Cal_Ent*, Fig. 2) for each soil property and validated
368 using validation samples for each soil order (*BD_Val_Ver*, *BD_Val_Alf*, *BD_Val_Inc* and
369 *BD_Val_Ent*, Fig. 2). The soil-order models for clay and CEC estimates built from Vertisols
370 and Alfisols and tested on the same soil order yielded acceptable predictions ($R^2_{val} > 0.50$,

371 RPIQ_{val} > 1.50), while the soil-order models built from Inceptisols and Entisols for clay and
372 CEC resulted in good predictions ($R^2_{\text{val}} > 0.70$, RPIQ_{val} > 3.00) (Table 3).

373 The soil-order models for sand estimation built from Alfisols and tested on the same
374 soil order yielded acceptable predictions ($R^2_{\text{val}} > 0.50$, RPIQ_{val} > 1.50), while those built from
375 Inceptisols and Entisols and tested on these same two soil orders yielded good predictions
376 ($R^2_{\text{val}} > 0.70$, RPIQ_{val} > 3.00) (Table 3). For Vertisol, the soil-order models for sand
377 estimation and tested on this same soil order yielded poor predictions ($R^2_{\text{val}} < 0.50$, RPIQ_{val} <
378 1.50) (Table 3). The soil-order models built from Entisols predicted silt content with
379 acceptable accuracy ($R^2_{\text{val}} > 0.50$, RPIQ_{val} > 1.50), and the three other soil-order models built
380 for silt estimation provided poor performances (Table 3). Regardless of the soil order, the
381 soil-order models for SOC yielded poor predictions ($R^2_{\text{val}} < 0.50$, RPIQ_{val} < 1.50) (Table 3).

382 In accordance with the R^2_{val} and RMSE_{val} values, these models calibrated from subsets
383 stratified by soil orders for clay prediction outperformed the regional model when applied to
384 each validation dataset of the corresponding soil order (Table 3). Similarly, the soil-order
385 models for Vertisols, Alfisols and Inceptisols performed better than the regional models for
386 the prediction of CEC. Although both regional and soil-order models performed well for the
387 prediction of the sand contents of Alfisols, Inceptisols and Entisols, with respect to RPIQ, the
388 soil-order model (RPIQ_{val} of 2.12) slightly outperformed the regional model (RPIQ_{val} of 2.04)
389 for Alfisols (Table 3). In addition, the regional models outperformed the soil-order models in
390 all other situations.

391 **Table 3.** Performance of regional and soil-order models (50 iterations) for the prediction of soil properties of different orders (standard deviation in parenthesis). (Models
392 that yielded R^2_{val} values from 0.50 to 0.70 are highlighted in bold. Models that yielded R^2_{val} values above 0.70 are highlighted in bold and underlined).

Properties	Model	Validation Dataset															
		<i>BD_val_Ver(26)</i>				<i>BD_val_Alf(72)</i>				<i>BD_val_Inc(48)</i>				<i>BD_val_Ent(8)</i>			
		R^2_{val}	<i>RMSE</i>	<i>bias</i>	<i>RPIQ</i>	R^2_{val}	<i>RMSE</i>	<i>bias</i>	<i>RPIQ</i>	R^2_{val}	<i>RMSE</i>	<i>bias</i>	<i>RPIQ</i>	R^2_{val}	<i>RMSE</i>	<i>bias</i>	<i>RPIQ</i>
	<i>val</i>	<i>val</i>	<i>val</i>		<i>val</i>	<i>val</i>	<i>val</i>		<i>val</i>	<i>val</i>	<i>val</i>		<i>val</i>	<i>val</i>	<i>val</i>		
clay (%)	regional models	0.48 (0.10)	9.09 (1.48)	-5.21 (1.41)	1.25 (0.26)	0.63 (0.06)	10.65 (0.91)	-0.49 (1.26)	1.95 (0.17)	0.78 (0.05)	8.52 (0.92)	1.25 (0.86)	3.24 (0.37)	0.84 (0.06)	8.85 (2.12)	4.77 (2.18)	3.43 (1.29)
	soil-order models	0.54 (0.11)	6.17 (0.93)	0.40 (1.15)	1.83 (0.31)	0.64 (0.06)	10.47 (0.71)	-0.54 (1.39)	1.98 (0.14)	0.79 (0.04)	8.42 (0.88)	-0.43 (1.18)	3.28 (0.37)	0.80 (0.08)	8.43 (1.98)	-0.13 (2.80)	3.63 (1.47)
CEC (cmol (+) kg ⁻¹)	regional models	0.58 (0.14)	12.69 (1.66)	-4.46 (1.64)	1.90 (0.29)	0.46 (0.09)	8.96 (1.42)	2.78 (1.08)	1.17 (0.18)	0.82 (0.04)	8.31 (0.77)	-1.45 (0.89)	3.88 (0.37)	0.72 (0.21)	9.88 (4.20)	3.12 (2.64)	3.04 (1.61)
	soil-order models	0.51 (0.14)	12.90 (1.58)	0.24 (2.08)	1.86 (0.21)	0.61 (0.05)	6.21 (0.69)	-0.01 (0.73)	1.67 (0.19)	0.83 (0.04)	7.94 (0.83)	0.11 (1.23)	4.07 (0.47)	0.68 (0.14)	9.45 (2.02)	-0.10 (2.69)	2.85 (0.94)
sand (%)	regional models	0.38 (0.13)	11.61 (2.25)	6.46 (1.98)	0.99 (0.30)	0.59 (0.06)	12.78 (1.00)	-1.21 (1.33)	2.04 (0.15)	0.79 (0.05)	10.32 (1.08)	-0.42 (1.28)	3.48 (0.38)	0.87 (0.06)	10.78 (2.01)	-3.42 (2.44)	4.31 (1.44)
	soil-order models	0.45 (0.13)	8.25 (1.52)	0.13 (1.97)	1.39 (0.32)	0.60 (0.06)	12.29 (0.76)	0.28 (1.32)	2.12 (0.14)	0.76 (0.05)	11.18 (1.07)	0.07 (0.14)	3.21 (0.34)	0.75 (0.08)	14.05 (2.60)	0.37 (4.45)	3.26 (0.97)
pH	regional models	0.43 (0.11)	0.53 (0.07)	-0.22 (0.08)	1.44 (0.23)	0.41 (0.08)	0.85 (0.06)	0.13 (0.07)	2.00 (0.13)	0.50 (0.08)	0.69 (0.07)	-0.09 (0.08)	1.47 (0.17)	0.30 (0.21)	0.76 (0.14)	0.15 (0.19)	1.93 (0.49)
	soil-order models	0.45 (0.11)	0.45 (0.06)	0.00 (0.08)	1.69 (0.27)	0.39 (0.08)	0.86 (0.07)	-0.01 (0.07)	1.99 (0.15)	0.41 (0.08)	0.76 (0.07)	0.02 (0.10)	1.34 (0.15)	0.12 (0.14)	0.79 (0.09)	-0.03 (0.13)	1.74 (0.26)
SOC (%)	regional models	0.32 (0.11)	0.21 (0.02)	0.01 (0.03)	1.34 (0.17)	0.16 (0.06)	0.24 (0.02)	0.01 (0.02)	1.52 (0.11)	0.30 (0.07)	0.24 (0.02)	-0.02 (0.02)	1.83 (0.17)	0.44 (0.30)	0.26 (0.14)	-0.05 (0.07)	1.56 (0.77)
	soil-order models	0.34 (0.10)	0.21 (0.02)	0.00 (0.03)	1.38 (0.17)	0.14 (0.06)	0.24 (0.02)	0.00 (0.02)	1.50 (0.12)	0.28 (0.08)	0.24 (0.02)	0.00 (0.03)	1.81 (0.17)	0.40 (0.28)	0.28 (0.10)	0.00 (0.10)	1.27 (0.48)
silt (%)	regional models	0.19 (0.12)	4.97 (0.66)	-1.18 (0.53)	1.50 (0.21)	0.31 (0.10)	5.44 (0.53)	1.30 (0.50)	1.20 (0.10)	0.50 (0.08)	5.29 (0.46)	-0.89 (0.56)	1.77 (0.18)	0.86 (0.07)	5.11 (1.02)	-1.78 (1.02)	3.35 (0.90)
	soil-order models	0.27 (0.13)	4.53 (0.63)	0.15 (0.69)	1.65 (0.24)	0.30 (0.13)	5.25 (0.55)	-0.24 (0.41)	1.25 (0.14)	0.41 (0.08)	5.62 (0.46)	0.00 (0.78)	1.67 (0.16)	0.53 (0.17)	7.84 (1.79)	0.48 (2.31)	2.24 (0.93)

393 4. Discussion

394 4.1. Predictions at the regional scale based on regional models

395 The soil properties which were successfully predicted based on regional models, were
396 characterized by i) a high variability (e.g., clay contents from 1.2 to 77.2% with a SD of 19%;
397 Table 2) and ii) either a spectral response due to physicochemical responses (e.g., clay which
398 is characterized by a absorption band at 2208 nm corresponding to the combination of OH
399 stretch and OH-Al bending modes, [Chabrillat et al., 2019](#)) or a correlation to one property
400 which was successfully predicted (e.g., sand which was correlated to clay, [Supplementary](#)
401 [Information 3](#)). These results are in accordance with the three rules defined by [Ben-Dor et al.](#)
402 [\(2002\)](#) and then [Gomez et al. \(2012a, b\)](#), presented in [Chabrillat et al. \(2019\)](#) and recalled in
403 our Introduction section. Conversely, soil properties characterized by a short variability of
404 values (e.g., SOC with a mean of 0.6% and SD of 1.1%, [Table 2](#)) were poorly predicted at the
405 regional scale by the regional models ([Fig. 5f](#)).

406 The accurate clay estimations might be due to the use of wavelengths in RF models
407 related to clay including the bands around 2208 nm corresponding to the combination of OH
408 stretch and OH-Al bending modes ([Chabrillat et al., 2002](#)). The accurate predictions of CEC
409 might be attributed to the correlation between CEC and clay and the large range of CEC
410 values at the regional scale ([Table 2](#)), as CEC does not have a primary response to spectral
411 reflectance ([Leone et al., 2012](#); [Xu et al., 2018](#)). Similar levels of performance were observed
412 for the various models for the prediction of clay, sand and CEC in the literature. [Ahmadi et](#)
413 [al. \(2021\)](#) stated that the mean coefficients of determination (R^2) for various Vis-NIR
414 prediction studies for sand and clay were 0.76 and 0.70, respectively. [Terra et al. \(2015\)](#)
415 emphasised that the promising results of models for the prediction of sand (R^2_{cal} from 0.85 to
416 0.90) and clay contents (R^2_{cal} from 0.85 to 0.88) may effectively replace the analysis of soil
417 particle size by conventional methods.

418 Silt content was predicted with reliable accuracy ($R^2_{\text{val}}=0.55$, $\text{RPIQ}_{\text{val}}=2.21$ and
419 $\text{RMSE}_{\text{val}}= 5.32\%$), which was in agreement with [Viscarra Rossel et al. \(2006\)](#). Additionally,
420 pH was predicted with reliable accuracy ($R^2_{\text{val}}=0.54$, $\text{RPIQ}_{\text{val}}=1.98$ and $\text{RMSE}_{\text{val}}= 0.75$),
421 which is difficult to explain because pH does not have any spectral response or correlation to
422 a property having a spectral response due to physical or chemical structures ([Supplementary](#)
423 [Information 3](#)). The low range for SOC content might be the cause of the poor prediction of
424 SOC ([Dalal and Henry, 1986](#)), which was confirmed with [Fig. 4](#), where no significant
425 absorption was observed near 500 and 800 nm ([Latz et al., 1984](#)).

426

427 **4.2. Predictions at the soil order scale based on regional models**

428 Based on regional models, the prediction performances obtained over each subset stratified
429 per soil order differed from those obtained at the regional scale ([Table 3](#) and [Fig. 5](#)). While
430 clay and sand contents may be considered correctly predicted at the regional scale ([Fig. 5a](#),
431 [b](#)), both soil properties were poorly predicted over Vertisols samples ([Table 3](#)), for which
432 these properties were characterized by a small range (SD of 8.75% and 10.6%, respectively,
433 [Table 2](#)) and thus do not follow the rule (1.3) stated by [Chabrillat et al. \(2019\)](#). Additionally,
434 while CEC may be considered correctly predicted at the regional scale ([Fig. 5c](#)), CEC was
435 poorly predicted for Alfisols samples ([Table 3](#)), which was characterized by a small CEC
436 range (SD of 9.8 cmol (+) kg^{-1} , [Table 2](#)) and thus does not follow the rule (1.3) stated by
437 [Chabrillat et al. \(2019\)](#).

438 So models based on the regional database for calibration can be considered as
439 providing high accuracy of some soil properties estimations when considering the regional
440 strategy in the validation step but modest accuracy of these same soil properties when
441 considering subsets stratified by soil order from the regional database in validation step.
442 These results are in accordance with [Gomez and Coulouma \(2018\)](#), who showed that while

443 their prediction models were accurate at a regional scale, the prediction model performances
444 at within-field scales depended on the specific soil property. As the estimation accuracy
445 appreciation is depending on the validation database, the appreciation of prediction
446 accuracies can be done both at regional and soil-order scale to reinforce the performance
447 analysis.

448

449 **4.3. Predictions at the soil order scale based on soil order models**

450 The soil-order models dedicated to Entisols and Inceptisols predict clay contents (R^2_{val} of
451 0.80 and 0.79, respectively, [Table 3](#)) with more accuracy than the soil-order models dedicated
452 to Vertisols (R^2_{val} of 0.54, [Table 3](#)), as the presence of smectite clay minerals and the high
453 moisture-holding capacity of Vertisols may reduce the relative spectral reflectance at 1300–
454 1400, 1800–1900, and 2200–2500 nm bands ([Baumgardner et al., 1985](#); [Babaeian et al.,](#)
455 [2015](#); [Demattê et al., 2017](#)). The prediction of CEC was on par with clay for different soil
456 orders, which might be due to a positive correlation between clay and CEC. The trends in
457 CEC prediction for the soil orders were similar to the trends in the correlation coefficients
458 between clay and CEC ([Supplementary Information 4-7](#)). The higher performances for sand
459 prediction ($R^2_{\text{val}} \geq 0.75$, [Table 3](#)) in Inceptisols and Entisols might be explained by the higher
460 sand content in these soils which are at the inception of soil development ([Santos et al.,](#)
461 [2013](#)). A relatively better prediction of silt content was achieved through a soil-order model
462 for Entisols, which might be attributed to the predominance of highly weatherable minerals in
463 these soils that alter their albedo ([Poppiel et al., 2018](#)).

464

465 **4.4. Regional model versus soil-order model**

466 For Vertisols, the soil-order models for clay and sand estimates significantly outperformed
467 the regional models ([Table 3](#)), while both the soil-order and regional models for other soil

468 property predictions provided a similar range of performances. For Alfisols, the soil-order
469 model for CEC estimates significantly outperformed the regional model (Table 3), while both
470 the soil-order and regional models for the other soil property predictions provided a similar
471 range of performances. Over Inceptisols, the regional models for pH and silt estimates
472 significantly outperformed the soil-order models (Table 3), while both the soil-order and
473 regional models for other soil property predictions provided a similar range of performances.
474 For Entisols, the regional models for CEC, sand and silt estimates significantly outperformed
475 the soil-order models (Table 3), while both the soil-order and regional models for the other
476 soil property predictions provided a similar range of performances.

477 Therefore, these results did not allow us to conclude whether a regional model or a
478 soil-order model is the best strategy for predicting different properties across different soils.
479 The literature is also not unanimous on this point, as some works have shown that regional
480 models outperform soil-order models (e.g., Vasques et al., 2010; Liu et al., 2018), while other
481 works have shown the opposite (e.g., Madari et al., 2005; McDowell et al., 2012). Therefore,
482 while our results did not enable any recommendations for choosing between a regional or
483 soil-order model, they highlight the risk of overestimating prediction accuracy at the soil-
484 order scale when figures of merit are based on a validation dataset built at the regional scale.

485

486 **5. Conclusion**

487 In the present study, the effectiveness of using Vis-NIR spectroscopy for the prediction of
488 soil properties was analyzed based on soil order knowledge in both calibration and validation
489 steps. While these results did not enable any recommendations for choosing between a
490 regional or soil-order model when validating on soil-order datasets, they highlighted the risk
491 of overestimating prediction accuracy at the soil-order scale when figures of merit are based
492 on a validation dataset built at a regional scale. As large soil spectral libraries are currently

493 highly developed, this work showed that soil-order knowledge may be useful to avoid
494 misestimating soil properties. In future, this work could be completed by an analysis of how
495 land use or other environmental covariates may be used to improve soil properties prediction
496 models.

497

498

499 **Acknowledgement**

500 The authors thank the Karnataka Watershed Development Department and the World Bank
501 for funding the Sujala III project. The authors thank the ATCHA, ANR-16-CE03-0006
502 project for supporting the work. The authors also thank Sebastien Troiano from INRAE,
503 UMR LISAH, for his help in setting up the spectral laboratory. The authors also acknowledge
504 Dr. Laurent Ruiz, Indo-French Cell for Water Sciences, Bangalore for his guidance in
505 developing the spectral library of Karnataka. The authors also thank Dr. Arti Koyal, CTO,
506 NBSS&LUP for helping with recording spectral data.

507

508

509 **Declaration of Competing Interest**

510 The authors declare that there are no known competing interests.

511

512 **References**

513 Ahmadi, A., Emami, M., Daccache, A., He, L., 2021. Soil Properties Prediction for Precision
514 Agriculture Using Visible and Near-Infrared Spectroscopy: A Systematic Review and
515 Meta-Analysis. *Agron.* 11, 433. <https://doi.org/10.3390/agronomy11030433>.

516 Asgari, N., Ayoubi, S., Demattê, J.A.M., Dotto, A.C., 2020. Carbonates and organic matter in
517 soils characterized by reflected energy from 350–25000 nm wavelength. *J. Mt. Sci.*
518 17, 1636–1651. <https://doi.org/10.1007/s11629-019-5789-9>

519 Babaeian, E., Homae, M., Vereecken, H., Montzka, C., Norouzi, A.A., van Genuchten,
520 M.T., 2015. A Comparative Study of Multiple Approaches for Predicting the Soil-
521 Water Retention Curve: Hyperspectral Information vs. Basic Soil Properties. *Soil Sci.*
522 *Soc. Am. J.* 79(4), 1043-1058. <https://doi.org/10.2136/sssaj2014.09.0355>.

523 Bao, Y., Meng, X., Ustin, S.L., Wang, X., Zhang, X., Liu, H., Tang, H., 2020. Vis-SWIR
524 spectral prediction model for soil organic matter with different grouping strategies.
525 *Catena* 195, 104703. <https://doi.org/10.1016/j.catena.2020.104703>.

526 Baumgardner, M.F., Silva, L.F., Biehl, L.L., Stoner, E.R., 1985. Reflectance properties of
527 soils. *Adv. Agron.* 38, 1–44. [doi:10.1016/S0065-2113\(08\)60672-0](https://doi.org/10.1016/S0065-2113(08)60672-0).

528 Bellon-Maurel, V., Fernandez-Ahumada, E., Palagos, B., Roger, J.M., McBratney, A., 2010.
529 Prediction of soil attributes by NIR spectroscopy. A critical review of chemometric
530 indicators commonly used for assessing the quality of the prediction. *Trends Anal.*
531 *Chem. (TRAC)* 29 (9), 1073–1081. <https://doi.org/10.1016/j.trac.2010.05.006>.

532 Bellon-Maurel, V., McBratney, A., 2011. Near-infrared (NIR) and mid-infrared (MIR)
533 spectroscopic techniques for assessing the amount of carbon stock in soils e Critical
534 review and research perspectives. *Soil Biol. Biochem.* 43(7), 1398-1410. [DOI:
535 10.1016/j.soilbio.2011.02.019](https://doi.org/10.1016/j.soilbio.2011.02.019).

536 Ben-Dor, E., 2002. Quantitative remote sensing of soil properties. *Adv. Agron.* 75, 173–243.
537 [doi:10.1016/S0065-2113\(02\)75005-0](https://doi.org/10.1016/S0065-2113(02)75005-0).

538 Ben-Dor, E., Patkin, K., Banin, A., Karnieli, A. 2002. Mapping of several soil properties
539 using DAIS-7915 hyperspectral scanner data: a case study over clayey soils in Israel.
540 *Int. J. Remote Sens.* 23, 1043–1062

541 Ben-Dor, E., Banin, A., 1995a. Near infrared analysis (NIRA) as a method to simultaneously
542 evaluate spectral featureless constituents in soils. *Soil Sci.* 159(4), 259–270.
543 <https://doi.org/10.1097/00010694-199504000-00005>.

544 Ben-Dor, E., Banin, A., 1995b. Near infrared analysis (NIRA) as a rapid method to
545 simultaneously evaluate several soil properties. *Soil Sci. Soc. Am. J.* 59, 364–372.
546 [10.2136/sssaj1995.03615995005900020014x](https://doi.org/10.2136/sssaj1995.03615995005900020014x)

547 Bilgili, A.V., van Es, H.M., Akbas, F., Durka, A., Hively, W.D., 2010. Visible near-infrared
548 reflectance spectroscopy for assessment of soil properties in a semi-arid area of
549 Turkey. *Arid Environ.* 74, 229–238. doi:10.1016/j.jaridenv.2009.08.011

550 Breiman, L., 2001. Random forests. *Mach. Learn.* 45, 5–32.
551 <https://doi.org/10.1023/A:1010933404324>.

552 Brown, D.J., 2007. Using a global VNIR soil-spectral library for local soil characterization
553 and landscape modeling in a 2nd-order Uganda watershed. *Geoderma* 140, 444–453.
554 [DOI:10.1016/j.geoderma.2007.04.021](https://doi.org/10.1016/j.geoderma.2007.04.021).

555 Chabrillat, S., Goetz, A.F.H., Krosley, L., Olsen, H.W., 2002. Use of hyperspectral images in
556 the identification and mapping of expansive clay soils and the role of spatial
557 resolution. *Remote Sens. Environ.* 82, 431–445. [https://doi.org/10.1016/S0034-](https://doi.org/10.1016/S0034-4257(02)00060-3)
558 [4257\(02\)00060-3](https://doi.org/10.1016/S0034-4257(02)00060-3).

559 Chabrillat, S., Gholizadeh, A., Neumann, C., Berger, D., Milewski, R., Ogen, Y., Ben-Dor, E.,
560 2019. Preparing a soil spectral library using the Internal Soil Standard (ISS) method:
561 Influence of extreme different humidity laboratory conditions. *Geoderma* 355,
562 113855. <https://doi.org/10.1016/j.geoderma.2019.07.013>.

563 Cozzolino, D., Morón, A., 2003. The potential of near-infrared reflectance spectroscopy to
564 analyse soil chemical and physical characteristics. *J. Agric. Sci.* 140(1), 65–71.
565 <https://doi.org/10.1017/S0021859602002836>.

566 Dalal, R.C., Henry, R.J., 1986. Simultaneous determination of moisture, organic carbon, and
567 total nitrogen by near infra-red reflectance spectrophotometry. *Crop Sci. Soc. Am.* 50,
568 120–123. <https://doi.org/10.2136/sssaj1986.03615995005000010023x>.

569 Davari, M., Karimi, S.A., Bahrami, H.A., Taher Hossaini, S.M., Fahmideh, S., 2021.
570 Simultaneous prediction of several soil properties related to engineering uses based on
571 laboratory Vis-NIR reflectance spectroscopy. *Catena* 197, 104987.
572 <https://doi.org/10.1016/j.catena.2020.104987>.

573 Delwiche, S.R., 2010. A graphical method to evaluate spectral preprocessing in multivariate
574 regression calibrations: Example with Savitzky-Golay filters and partial least squares
575 regression. *Appl. Spectrosc.* 64, 73–82.
576 <https://doi.org/10.1366/000370210790572007>.

577 Demattê, J.A., Campos, R.C., Alves, M.C., Fiorio, P.R., Nanni, M.R., 2004. Visible–NIR
578 reflectance: a new approach on soil evaluation. *Geoderma* 121, 95-112.
579 <https://doi.org/10.1016/j.geoderma.2003.09.012>

580 Demattê, J.A.M., Horák-Terra, I., Beirigo, R.M., Terra, F. da S., Marques, K.P.P., Fongaro,
581 C.T., Silva, A.C., Vidal-Torrado, P., 2017. Genesis and properties of wetland soils by
582 VIS-NIR-SWIR as a technique for environmental monitoring. *J. Environ. Manage.*
583 197, 50–62. <https://doi.org/10.1016/j.jenvman.2017.03.014>.

584 Dharumarajan, S., Lalitha, M., Gomez, C., Vasundhara, R., Kalaiselvi, B., Hegde, R. 2022.
585 Prediction of soil hydraulic properties using VIS-NIR spectral data in semi- arid
586 region of Northern Karnataka Plateau. *Geoderma Reg.*
587 <https://doi.org/10.1016/j.geodrs.2021.e00475>.

588 Efron, B., Tibshirani, R., 1993. *An Introduction to the Bootstrap*. Chapman and Hall, London,
589 UK.

590 Farifteh, J., Meer, F.D., Meijde, M.V., Atzberger, C., 2008. Spectral characteristics of salt-
591 affected soils: A laboratory experiment. *Geoderma* 145, 196-206.
592 <https://doi.org/10.1016/j.geoderma.2008.03.011>.

593 Ghasemi, J. B., Tavakoli, H., 2013. Application of random forest regression to spectral
594 multivariate calibration. *Anal. Methods* 5, 1863-1871.
595 <https://doi.org/10.1039/C3AY26338J>.

596 Gogé, F., Joffre, R., Jolivet, C., Ross, I., Ranjard, L., 2012. Optimization criteria in sample
597 selection step of local regression for quantitative analysis of large soil NIRS database.
598 *Chemom. Intell. Lab. Syst.* 110 (1), 168–176.

599 Gogé, F., Gomez, C., Jolivet, C., Joffre, R., 2014. Which strategy is best to predict soil
600 properties of a local site from a national Vis–NIR database? *Geoderma* 213, 1–9.
601 <http://dx.doi.org/10.1016/j.geoderma.2013.07.016>.

602 Gomez, C., Coulouma, G., 2018. Importance of the spatial extent for using soil properties
603 estimated by laboratory VNIR/SWIR spectroscopy: Examples of the clay and calcium
604 carbonate content, *Geoderma* 330, 244–253.
605 <https://doi.org/10.1016/j.geoderma.2018.06.006>.

606 Gomez, C., Lagacherie, P., Bacha, S., 2012b. Using Vis–NIR hyperspectral data to map
607 topsoil properties overbare soils in the Cap Bon region, Tunisia. In: *Digital soil
608 assessments and beyond—proceedings of the fifth global workshop on digital soil
609 mapping*, pp 387–392.

610 Gomez, C., Lagacherie, P., Coulouma, G., 2008. Continuum removal versus PLSR method
611 for clay and calcium carbonate content estimation from laboratory and airborne
612 hyperspectral measurements. *Geoderma* 148, 141–148.
613 <https://doi.org/10.1016/j.geoderma.2008.09.016>.

614 Gomez, C., Lagacherie, P., Coulouma, G., 2012a. Regional predictions of eight common soil
615 properties and their spatial structures from hyperspectral Vis–NIR data. *Geoderma*
616 189–190, 176–185. <http://dx.doi.org/10.1016/j.geoderma.2012.05.023>.

617 Guerrero, C., Zornoza, R., Gómez, I., Mataix-Beneyto, J., 2010. Spiking of NIR regional
618 models using samples from target sites: effect of model size on prediction accuracy.
619 *Geoderma* 158, 66–77.

620 Gupta, A., Hitesh B. V., Das, B. S., Choubey, A. K., 2018. Local modeling approaches for
621 estimating soil properties in selected Indian soils using diffuse reflectance data over
622 visible to near-infrared region. *Geoderma* 325, 59–71.
623 <https://doi.org/10.1016/j.geoderma.2018.03.025>

624 Hedley, C., Roudier, P., Maddi, L., 2015. VNIR Soil Spectroscopy for Field Soil Analysis.
625 *Commun. Soil Sci. Plant Anal.* 46, 104–121. DOI: [10.1080/00103624.2014.988582](https://doi.org/10.1080/00103624.2014.988582).

626 Hobley, E.U., Prater, I., 2019. Estimating soil texture from vis–NIR spectra. *Eur. J. Soil Sci.*
627 70, 83–95, [10.1111/ejss.12733](https://doi.org/10.1111/ejss.12733)

628 Hegde, R., Niranjana, K. V., Srinivas, S., Danorkar, B. A., Singh. S. K., 2018. Site-specific
629 land resource inventory for scientific planning of Sujala watersheds in Karnataka.
630 *Current Sci.* 115(4), 645–652. <http://dx.doi.org/10.18520/cs/v115/i4/644-652>.

631 Jackson, M.L., 1973. *Soil Chemical Analysis*. Prentice Hall of India Pvt. Ltd. New Delhi.

632 Jaconi, A., Vos, C., Don, A., 2019. Near infrared spectroscopy as an easy and precise method
633 to estimate soil texture. *Geoderma* 337, 906–913.
634 <https://doi.org/10.1016/j.geoderma.2018.10.038>

635 Latz, K., Wesimiller, R.A., Van Scoyoc, G.E., Baumgardner, M.F., 1984. Characteristic
636 variation in spectral reflectance of selected eroded Alfisols. *Soil Sci. Soc. Am. J.* 48,
637 1130–1134. <https://doi.org/10.2136/sssaj1984.03615995004800050035x>.

638 Leone, A.P., Viscarra-Rossel, R.A., Amenta, P., Buondonno, A., 2012. Prediction of soil
639 properties with PLSR and Vis-NIR spectroscopy: application to Mediterranean soils
640 from Southern Italy. *Curr. Analy. Chem.* 8, 283–299.
641 <https://doi.org/10.2174/157341112800392571>.

642 Liu, Y., Shi, Z., Zhang, G., Chen, Y., Li, S., Hong, Y., Shi, T., Wang, J., Liu, Y. 2018.
643 Application of spectrally derived soil type as ancillary data to improve the estimation
644 of soil organic carbon by using the Chinese soil Vis-NIR Spectral Library. *Remote*
645 *Sen.* 10(11), 1747. <https://doi.org/10.3390/rs10111747>.

646 Lobsey, C. R., Viscarra Rossel, R. A., Roudier, P., Hedley, B., 2017. RS-local data-mines
647 information from spectral libraries to improve local calibrations. *Eur. J. Soil Sci.* 68,
648 840–852. doi: 10.1111/ejss.12490

649 Madari, B.E., Reeves, J.B., Coelho, M.R., Machado, P.L., De-Polli, H., Coelho, R.M.,
650 Benites, V.M., Souza, L.F., McCarty, G.W., 2005. Mid and near-infrared
651 spectroscopic determination of carbon in a diverse set of soils from the Brazilian
652 national soil collection. *Spectrosc. Lett.* 38, 721–740.
653 <https://doi.org/10.1080/00387010500315876>.

654 McBride, M. B. 2022. Estimating soil chemical properties by diffuse reflectance
655 spectroscopy: Promise versus reality. *European J. Soil Sci.* 73, e13192.
656 <https://doi.org/10.1111/ejss.13192>.

657 McDowell, M. L., Bruland, G.L., Deenik, J.L., Grunwald, S., 2012. Effects of subsetting by
658 carbon content, soil order, and spectral classification on prediction of soil total carbon
659 with diffuse reflectance spectroscopy. *Appl. Environ. Soil Sci.*
660 <https://doi.org/10.1155/2012/294121>.

661 Morellos, A., Pantazi, X.-E., Moshou, D., Alexandridis, T., Whetton, R., Tziotzios, G.,
662 Wiebenson, J., Bill, R., Mouazen, A. M., 2016. Machine learning based prediction of

663 soil total nitrogen, organic carbon and moisture content by using Vis-NIR
664 spectroscopy. *Biosyst. Eng.* 152, 104–116.
665 <http://dx.doi.org/10.1016/j.biosystemseng.2016.04.018>.

666 Naibo, G., Ramon, R., Pesini, G., Moura-Bueno, J.M., Barros, C.A., Caner, L., Silva, Y.J.,
667 Minella, J.P., dos Santos, D.R., Tiecher, T., 2022. Near-infrared spectroscopy to
668 estimate the chemical element concentration in soils and sediments in a rural
669 catchment. *Catena* 213, 106145. <https://doi.org/10.1016/j.catena.2022.106145>.

670 Nawar, S., Mouazen, A., 2019. On-line vis-NIR spectroscopy prediction of soil organic
671 carbon using machine learning. *Soil Till. Res.* 190, 120–127.
672 <https://doi.org/10.1016/j.still.2019.03.006>.

673 Nawar, S., Mouazen, A., 2017. Predictive performance of mobile vis-near infrared
674 spectroscopy for key soil properties at different geographical scales by using spiking
675 and data mining techniques. *Catena* 151, 118–129.
676 <https://doi.org/10.1016/j.catena.2016.12.014>.

677 NBSS&LUP, 1998. Soils of Karnataka for Optimising Land Use. NBSS Publ., 47b. ISBN:81-
678 85460-45-0.

679 Naimi, S., Ayoubi, S., Di Raimo, L. A. D. L., Dematte, J. A. M., 2022. Quantification of
680 some intrinsic soil properties using proximal sensing in arid lands: Application of Vis-
681 NIR, MIR, and pXRF spectroscopy. *Geoderma Reg.* 28, e00484.
682 <https://doi.org/10.1016/j.geodrs.2022.e00484>

683 Nocita, M., Stevens, A., Toth, G., Panagos, P., vanWesemael, B., Montanarella, L., 2014.
684 Prediction of soil organic carbon content by diffuse reflectance spectroscopy using a
685 local partial least square regression approach. *Soil Biol. Biochem.* 68, 337–347.

686 Ng, W., Minasny, B., Jeon H., McBratney, A., 2022. Mid-infrared spectroscopy for accurate
687 measurement of an extensive set of soil properties for assessing soil functions. *Soil*
688 *Security* 100043, <https://doi.org/10.1016/j.soisec.2022.100043>.

689 Peng, Y., Knadel, M., Gislum, R., Deng, F., Norgaard, T., de Jonge, L.W., Moldrup, P.,
690 Greve, M.H., 2013. Predicting soil organic carbon at field scale using a national soil
691 spectral library. *J. Near Infrared Spectrosc.* 21, 213–222.

692 Pinheiro, E. F. M., Ceddia, M. B., Clingensmith, C. M., Grunwald, S., Vasques, G. M., 2017.
693 Prediction of Soil Physical and Chemical Properties by Visible and Near-Infrared
694 Diffuse Reflectance Spectroscopy in the Central Amazon. *Remote Sens.* 9 (4).
695 [DOI:10.3390/rs9040293](https://doi.org/10.3390/rs9040293).

696 Poppiel, R.R., Lacerda, M.P.C., Oliveira Junior, M.P., Demattê, J.A.M., Romero D.J., Sato,
697 M.V., Almeida Júnior, L.R., Cassol, L.F.M., 2018. Surface spectroscopy of Oxisols,
698 Entisols and Inceptisol and relationships with selected soil properties. *Rev. Bras.*
699 *Ciênc. Solo* 42, e0160519.

700 Richards, L. A., 1954. Diagnosis and improvement of saline and alkali soils. USDA
701 Handbook, 60. USDA, Washington. D.C., USA

702 Sankey, J. B., Brown, D. J., Bernard, M. L., Lawrence, R. L., 2008. Comparing local vs.
703 global visible and near-infrared (visnir) diffuse reflectance spectroscopy (DRS)
704 calibrations for the prediction of soil clay, organic C and inorganic C. *Geoderma* 148,
705 149-158. <http://dx.doi.org/10.1016/j.geoderma.2008.09.019>.

706 Santos, H.G., Jacomine, P.K.T., Anjos, L.H.C., Oliveira, V.A., Lumbreras, J.F., Coelho,
707 M.R., Almeida, J.A., Cunha, T.J.F., Oliveira, J.B., 2013. Sistema brasileiro de
708 classificação de solos. 3a ed. Brasília, DF: Embrapa Solos.

709 Shepherd, K.D., Walsh, M. G., 2002. Development of reflectance spectral libraries for
710 characterization of soil properties. *Soil Sci. Soc. Am. J.* 66, 988–998.
711 <https://doi.org/10.2136/sssaj2002.9880>.

712 Shi, Z., Ji, W., Viscarra Rossel, R.A., Chen, S., Zhou, Y., 2015. Prediction of soil organic
713 matter using a spatially constrained local partial least squares regression and the
714 Chinese vis–NIR spectral library. *Eur. J. Soil Sci.* 66, 679–687.

715 Soil Survey Staff, 2014. Keys to soil taxonomy. 12th ed. Washington, DC: United States
716 Department of Agriculture, Natural Resources Conservation Service.

717 Srivastava, R., Prasad, J., Saxena, R.K., 2004. Spectral reflectance properties of some shrink-
718 swell soils of Central India as influenced by soil properties. *Agropedology* 14, 45-54.

719 Stenberg, B., Viscarra Rossel, R.A., Mouazen, A.M., Wetterlind, J., 2010. Visible and near
720 infrared spectroscopy in soil science. *Adv. Agron.* 107, 163–215.
721 [https://doi.org/10.1016/S0065-2113\(10\)07005-7](https://doi.org/10.1016/S0065-2113(10)07005-7).

722 Stevens, A., Nocita, M., Tóth, G., Montanarella, L., van Wesemael, B., 2013. Prediction of
723 soil organic carbon at the European scale by visible and near infrared reflectance
724 spectroscopy. *PLoS One* 8, e66409

725 Terra, F.S., Demattê, J.A.M., Rossel, R.A.V., 2015. Spectral libraries for quantitative
726 analyses of tropical Brazilian soils: Comparing Vis–NIR and mid-IR reflectance data.
727 *Geoderma* 255–256, 81-93. <http://doi.org/10.1016/j.geoderma.2015.04.017>.

728 Vasques, G.M., Grunwald, S.J.O.S., Sickman, J.O., 2008. Comparison of multivariate
729 methods for inferential modeling of soil carbon using visible/near-infrared spectra.
730 *Geoderma* 146 (1), 14–25.

731 Vasques, G.M., Grunwald, S., Harris, W.G., 2010. Spectroscopic models of soil organic
732 carbon in Florida, USA. *J. Environ. Qual.* 39, 923–934.
733 <https://doi.org/10.2134/jeq2009.0314>.

734 Veum, K.S., Sudduth, K.A., Kremer, R.J., Kitchen, N.R., 2015. Estimating a Soil Quality
735 Index with VNIR Reflectance Spectroscopy. *Soil Sci. Soc. Am. J.* 79, 637-649.
736 <https://doi.org/10.2136/sssaj2014.09.0390>.

737 Viscarra Rossel, R.A., Behrens, T., 2009. Using data mining to model and interpret soil
738 diffuse reflectance spectra. *Geoderma* 158 (1), 46–54.

739 Viscarra Rossel, R.A., Walvoort, D.J.J., McBratney, A.B., Janik, L.J. Skjemstad, J.O., 2006.
740 Visible, near infrared, mid infrared or combined diffuse reflectance spectroscopy for
741 simultaneous assessment of various soil properties. *Geoderma* 131, 59–75.
742 <https://doi.org/10.1016/j.geoderma.2005.03.007>.

743 Viscarra Rossel, R.A., Webster, R., 2011. Discrimination of Australian soil horizons and
744 classes from their visible–near infrared spectra. *Eur. J. Soil Sci.* 62, 637–647.
745 <https://doi.org/10.1111/j.1365-2389.2011.01356.x>.

746 Viscarra Rossel, R.A., Behrens, T., Ben-Dor, E., Brown, D.J., Demattê, J.A.M., Shepherd,
747 K.D. et al. 2016. A global spectral library to characterize the world’s soil. *Earth Sci.*
748 *Rev.* 155, 198–230.

749 Walkley, A., Black, I.A. 1934. An estimation of the method for determining soil organic
750 matter and a proposed modification of the chromic acid titration method. *Soil Sci.* 37,
751 29-38.

752 Wetterlind, J., Stenberg, B., 2010. Near-infrared spectroscopy for within-field soil
753 characterization: Small local calibrations compared with national libraries spiked with
754 local samples. *Eur. J. Soil Sci.* 61, 823–843. [https://doi.org/10.1111/j.1365-](https://doi.org/10.1111/j.1365-2389.2010.01283.x)
755 [2389.2010.01283.x](https://doi.org/10.1111/j.1365-2389.2010.01283.x).

756 Xu, S., Shi, X., Wang, M., Zhao, Y., 2016. Effects of subsetting by parent materials on
757 prediction of soil organic matter content in a hilly area using Vis–NIR spectroscopy.
758 *PLoS ONE* 11(3): e0151536 Zeng, R., Zhao, Y.-G., Li, D.-C., Wu, D.-W., Wei, C.-L.,

759 Zhang, G.-L., 2016. Selection of “Local” models for prediction of soil organic matter
760 using a regional soil Vis-NIR Spectral Library. *Soil Sci.* 181, 13–19.
761 <http://dx.doi.org/10.1097/SS.0000000000000132> .

762 Zeng, R., Zhao, Y.-G., Li, D.-C., Wu, D.-W., Wei, C.-L., Zhang, G.-L. 2016. Selection of
763 “Local” models for prediction of soil organic matter using a regional soil Vis-NIR
764 Spectral Library. *Soil Sci.* 181, 13–19.
765 <http://dx.doi.org/10.1097/SS.0000000000000132>.

766 Zeraatpisheh, M., Ayoubi, S., Mirbagheri, Z., Mosaddeghi, M. R., Xu, M., 2021. Spatial
767 prediction of soil aggregate stability and soil organic carbon in aggregate fractions
768 using machine learning algorithms and environmental variables. *Geoderma Reg.* 27,
769 e00440. <https://doi.org/10.1016/j.geodrs.2021.e00440>

770

771